Nonlinear Analyses of the Medieval “Ponte del Diavolo”, Borgo a Mozzano, Italy

A. De Falco[1], M. Girardi[2] and D. Pellegrini[1]
[1]Department of Energy, Systems, Territory and Construction Engineering University of Pisa, Italy
[2]Institute of Information Science and Technologies “A. Faedo” ISTI-CNR, Pisa, Italy

Abstract

Structural analyses are particularly difficult to conduct on masonry constructions due to the lack of knowledge of such materials’ mechanical properties. However, one well-established peculiar characteristic of masonry is its radically different behavior under tensile and compressive stresses. A suitable constitutive equation has been developed that models masonry as an isotropic elastic non-linear material with zero tensile strength and either infinite or bounded compressive strength. This constitutive equation, which is known as the masonry-like model, has been implemented in the finite element code NOSA-ITACA, which has been successfully applied to the static analysis of several historical masonry buildings as well as the dynamic analysis of masonry pillars, beams and towers.
In this work the Maddalena bridge, known as the "Devil's Bridge" (“Ponte del Diavolo”), on the Serchio river in Borgo a Mozzano (Italy) is studied. The paper presents several structural analyses performed through the NOSA-ITACA code by means of finite element models composed of plane or three-dimensional elements. Initially, the structural behavior of the bridge under permanent loads is investigated via non-linear static analysis. Then, a nonlinear dynamic analysis is performed using a time-dependent three-dimensional acceleration recorded during the earthquake that occurred in the nearby “Lunigiana” area on June 21, 2013. The results are analyzed and the differences between the linear and nonlinear behaviors are highlighted.

Keywords: masonry bridges, dynamic analysis, nonlinear elasticity, numerical methods, seismic response.

1 Introduction

The Maddalena bridge in Borgo a Mozzano, also known as the Devil’s Bridge, is one of the most fascinating medieval bridges in Italy (Figure 1). Although its exact origins are unknown, the bridge can be dated back to around the 11th century, when it represented a fundamental road infrastructure connecting some major routes in the Italian territory [1]. This sandstone and limestone masonry construction crosses the Serchio river for a total length of about one hundred meters, following the path of rocky outcrops, and deviating over fifteen degrees from the direction perpendicular to the river. The bridge is made up of four semicircular arches having clear spans of 38 m, 14.5 m, 10.5 m and 8.5 m, and a transverse section between 3.5 m and 3.7 m

wide. The arch barrel of the main span, which is just one meter high at the key, has a perfectly circular intrados profile with radius of 19 m. The three piers in the riverbed are braced by triangular shaped buttresses oriented along the direction of the river flow, on the upstream side, while the pier between the second and the third arch has a trapezoidal buttress, on the downstream side.

Figure 1. The Maddalena Bridge in Borgo a Mozzano (LU): a) View of the lateral side with empty riverbed. b) Downstream side. c) Upstream side.

Although the original structure of the bridge has certainly undergone a number of alterations over the centuries (due to local collapses), the most evident modification was performed in the early 1900s, when the bridge ceased to perform its original function: the right abutment was partially demolished in order to allow for construction of a new railway line. To this end, a new 5 m span arch straddling the railway and an "S" shaped ramp were built on the right bank. Later, during the 1950s, a hydraulic barrier for energy production was built downstream of the bridge and caused the formation of a reservoir that changed the profile of the bridge (Figures 1b and 1c). The Maddalena bridge has become the most representative monument of the Serchio valley today.

In the following we report on static and dynamic structural analyses performed in order to assess the structure's safety level. In particular, by means of finite element models of varying complexity, it has been possible to determine the internal forces induced by the structure's self-weight and during an earthquake. All analyses have been conducted by modeling masonry as a nonlinear elastic material with null tensile strength and limited compressive strength.

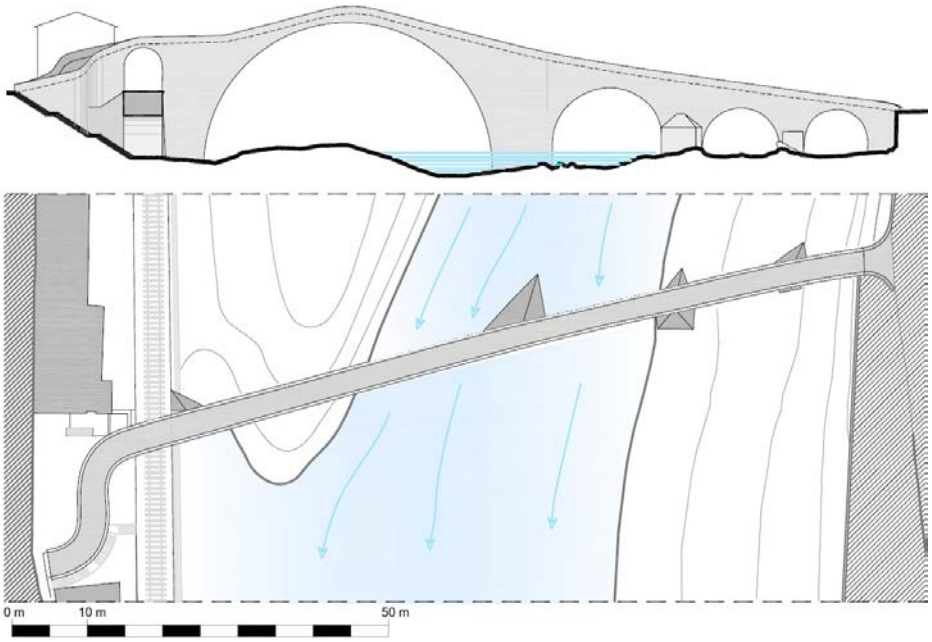

Figure 2. Elevation and plan of the bridge.

2 Structural analysis of the bridge

2.1 The NOSA-ITACA finite-element code

NOSA-ITACA is freeware/open-source software for computational mechanics [2], distributed with the aim of disseminating the use of mathematical models and numerical tools in the field of Cultural Heritage. NOSA-ITACA is the result of the integration of the finite element code NOSA [3] into the open-source SALOME platform [4].

The finite element code NOSA (NOn-Linear Structural Analysis) has been developed by the Mechanics of Materials and Structures Laboratory of the ISTI-CNR with the aim of testing new constitutive models for materials. It has moreover been applied to checking the algorithms for integrating the equations of motion, as well as to other numerical techniques for solving structural engineering problems. The development of NOSA began in 1980 and has continued over the ensuing years along the research lines of the Lab.

Over recent decades, constitutive models and calculation techniques have become available that enable a realistic description of the static behavior of masonry structures. Several studies [3], [5], [6] have led to a better understanding of the constitutive equation of materials not withstanding tension, known in the literature as *masonry-like* or *no-tension* materials. Within this framework, masonry is modeled as a nonlinear elastic material with zero tensile strength and infinite or bounded compressive strength.

In order to study real problems, the equilibrium problem of masonry structures can be solved via the finite element method. To this end, suitable numerical techniques

have been developed [3] based on the Newton-Raphson method for solving the nonlinear system obtained by discretizing the structure into finite elements. Their application requires that the derivative of the stress with respect to the strain be known explicitly, as this is needed in order to calculate the tangent stiffness matrix. The numerical method studied has therefore been implemented into the NOSA code to enable determination of the stress state and the presence of any cracking. It can moreover be applied to modeling needed restoration and reinforcement operations on constructions of particular architectural interest.
Finally, numerical solution of dynamic problems requires direct integration of the equations of motion [7]. With an aim to solving such problems, the Newmark method has been implemented within NOSA in order to perform the integration with respect to time of the system of ordinary differential equations obtained by discretizing the structure into finite elements. Moreover, the Newton-Raphson scheme, needed to solve the nonlinear algebraic system obtained at each time step, has been adapted to the dynamic case.
The code has been applied to the analysis of arches and vaults [3], as well as to some buildings of historical and architectural interest. Development of the code has been made possible through the funding of the CNR, the Italian Ministry of Universities and Research and the Region of Tuscany (NOSA-ITACA project). Within the framework of this project, the NOSA code has been substantially modified and equipped with new finite elements, thus enhancing its application capabilities. An efficient implementation of numerical methods for constrained eigenvalue problems, which enables conducting modal structural analyses while taking into account the features of master-slave constraints (tying or multipoint constraints), has been embedded in NOSA. Such implementation is based on open-source packages for managing matrices in sparse format in order to improve convergence [8]
Recent applications of the NOSA-ITACA code are described in [9], [10], [11]. Some examples of dynamic analyses conducted via the NOSA-ITACA code can be found in [12], [13], [14].
For this study, NOSA-ITACA has been applied to model the structural behavior of the Maddalena bridge. Two finite element models have been defined using eight-node isoparametric brick elements with bilinear interpolating shape functions (Model 1) and four-node thick shell elements with linear interpolating functions (Model 2). The two models have been used to evaluate the static behavior of the bridge under its self-weight. Then, Model 2 was employed to study the dynamic behavior of the bridge. For all analyses, the material self-weight alone was considered, as it is by far the most relevant load in the structure and an essential factor for stability safety. For the dynamic analyses, viscous damping has been considered, with a damping ratio $\xi = 5\%$. The damping matrix of the structure has been calculated in accordance with the Rayleigh assumption [15].

2.2 The bridge under its self-weight

The three-dimensional model (Model 1) used to study the structure under its own weight alone is shown in Figure 3. It models the structure without the masonry parapet, whose presence has been simulated by means of vertical distributed loads

and concentrated masses. The mesh consists of 30156 brick elements and 38626 nodes, for a total number of 115878 degrees of freedom. The base nodes are restrained in all directions, while the lateral nodes of the spandrels are restrained only in the two horizontal directions (see Figure 1). In particular, in order to simulate the effect of the railway embankment close to the bridge structure, the nodes of the right ramp and those in the proximity of the railway have been restrained in the x and y directions. Likewise, the lateral nodes in the proximity of the left spandrel are also assumed to be restrained in the x and y directions, in order to account for the presence of the soil on the river bank.
As no knowledge of the internal composition of the masonry is available, the material has been modeled as homogeneous, however differentiating the more compact and resistant material of the arch barrel. The assumed material characteristics are listed in Table 1.

Masonry type	Elastic modulus, E [MPa]	Unit weight, γ [kN/m^3]	Poisson ratio, ν
Sandstone masonry (arch barrel)	8000	24	0.2
Limestone (remaining structure)	3000	24	0.2

Table 1. Mechanical properties of the material used in the models.

The model reached equilibrium convergence with zero material tensile strength. Figure 4 shows the results in terms of minimum principal stresses. The absolute maximum compressive stress at the base of the principal arch attains a value of 1.3 MPa, which is considerably lower than the limit value for the material. One noteworthy finding is that the main arch barrel is the most heavily loaded element and shows a stress pattern different from what was expected. In particular, it exhibits compressive stresses on the intrados of the crown and on the extrados of two sections located symmetrically at about 17° from the central vertical axis. The reason for this unusual structural behavior of the main arch is essentially due to the particular shape of the profiles near the keystone, rather than to the material constitutive law. In fact, the same behavior has been found, in terms of both stress distribution and deformed shape, in the linear elastic analysis as well. In addition, a construction sequence has been modeled by changing some internal constraints at different load increments, performed under different assumptions on scaffolding and centering types. This analysis revealed no relevant changes in the stress regime and resulted in similar final deformations.
Figure 5 depicts the distribution of the maximum principal fracture strains; the arrangement of the fracture strains at the intrados of the main span arch barrel confirms what was first observed for the principal stresses. Another region in which fracture strains are located can be discerned at the intrados of the second span.
The simplified model (Model 2) is reported in Figure 6. It models the structure in its middle plane and is constituted by 5531 plane thick shell elements and 5861 nodes, having overall 35166 degrees of freedom. As for Model 1, the base nodes are restrained in all directions, while the boundary lateral nodes are free in the vertical direction and restrained in both horizontal directions. All boundary nodes are fully

restrained with respect to out-of-plane rotations. The material characteristics are those reported in Table 1.
The results in terms of minimum principal stresses are quite similar to those obtained for Model 1. In particular, Figure 6 clearly highlights the stress pattern in the main arch, while Figure 7 shows the corresponding vertical displacement map.

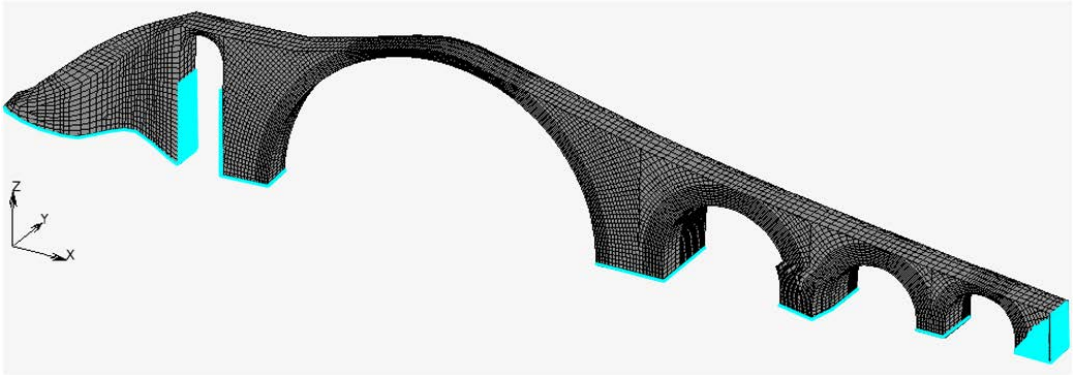

Figure 3. Model 1: the brick elements model. Restrained nodes are highlighted.

Sensitivity analysis was also performed by changing the material characteristics assumed in the calculations on the main arch barrel. The resulting original representation of the line of thrust on the principal arch ring is shown in Figure 8. Two cases are reported: one for a Young's modulus of 8000 MPa in the arch barrel (blue line), and the other for a homogeneous elastic modulus of 3000 MPa (red line) throughout the structure. The thrust intensity values on the transverse section of the arch ring are reported in the radial direction. The thrust reaches nearly 2000 kN at the crown and 2800 kN in the sections symmetrically located at 30° of the vertical central axis of the arch. The substantial permanence of the compression values near the crown is evident in both cases. It can also be seen that the massive lateral piers are able to ensure full stability of the central arch, even in the absence of the adjacent structures. Such an arrangement, typical of Roman bridges, avoids arch collapse in the event of failure of adjacent ones.

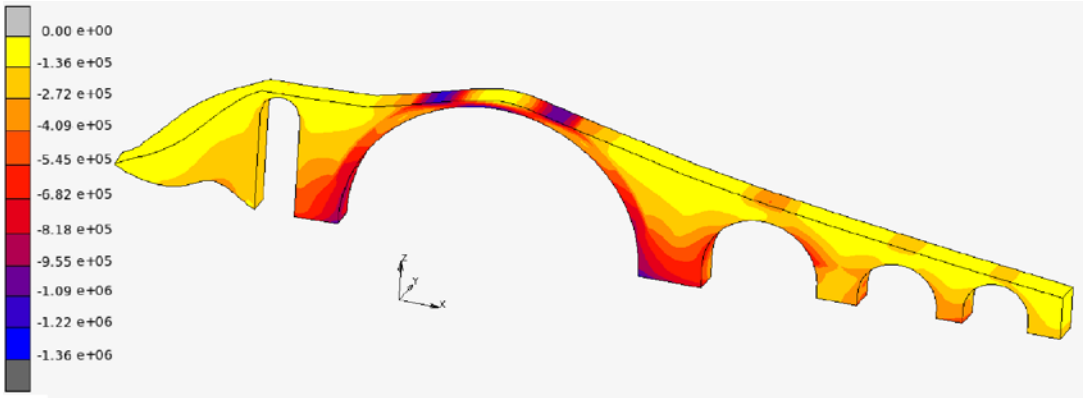

Figure 4. Minimum principal values of the stress tensor in the model 1 [N/m^2].

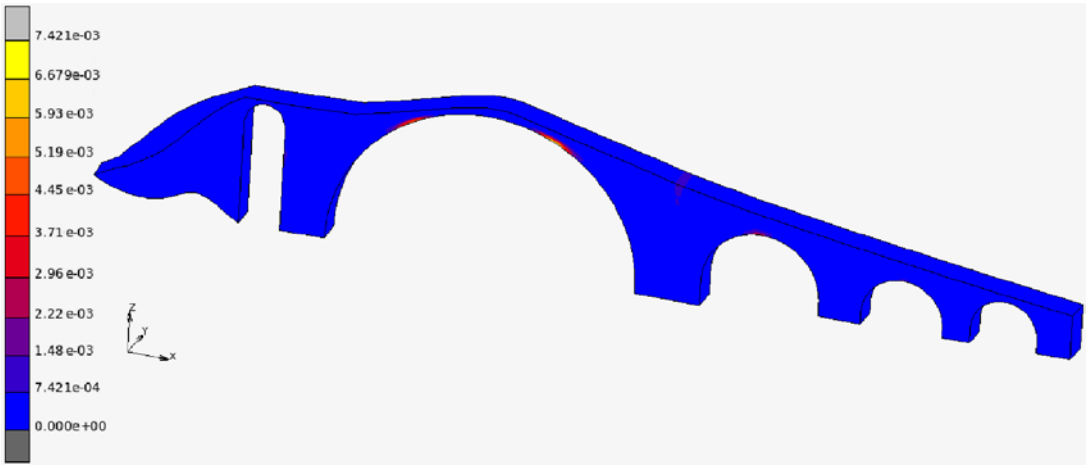

Figure 5. Maximum principal fracture strains in Model 1.

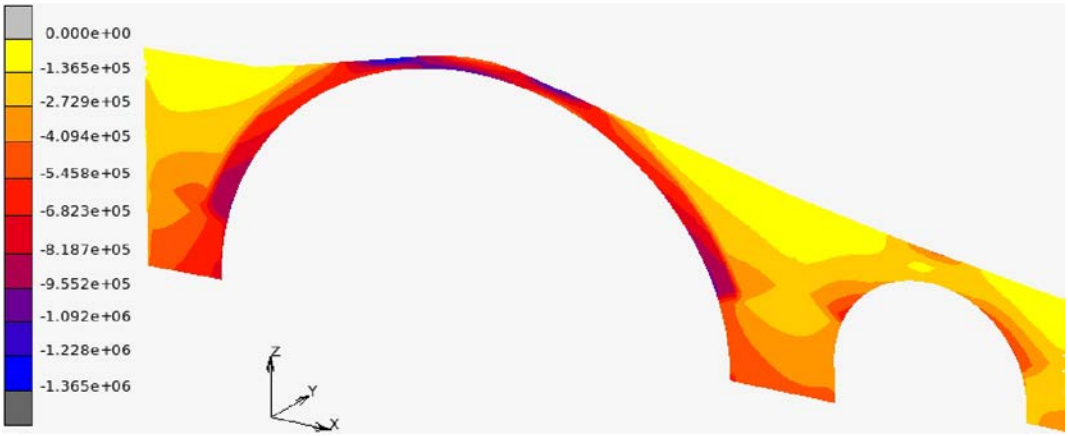

Figure 6. Minimum principal values of the stress tensor in the shell model (Model 2) [N/m^2] - main arch magnified.

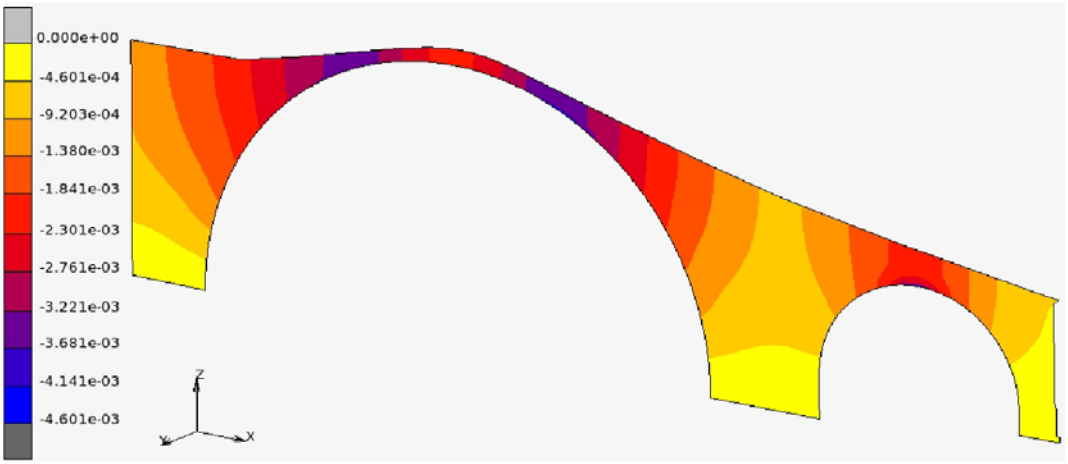

Figure 7. Model 2: map of *z* - displacements [m] - main arch magnified.

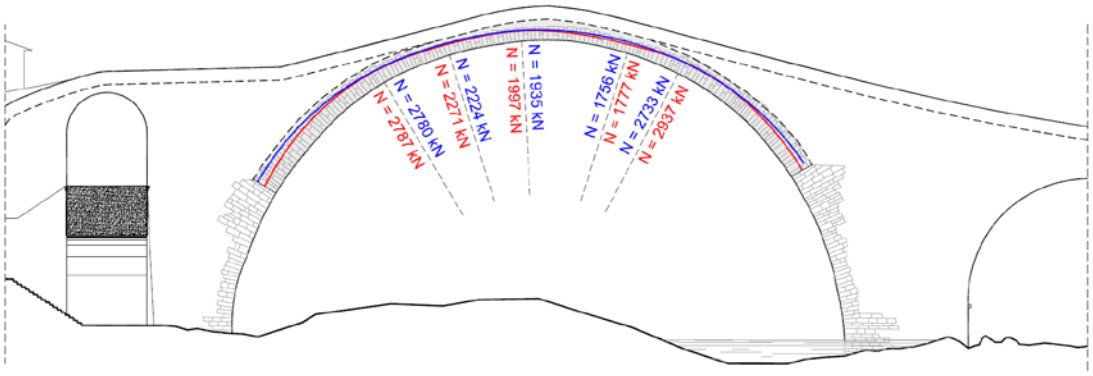

Figure 8. Lines of thrust on the main arch for different values of Young's modulus of the arch ring material: E = 8000 MPa (blue line), E = 3000 MPa (red line).

2.3 Dynamic analyses

2.3.1 Modal analysis

A preliminary modal analysis was performed in order to ascertain the fundamental frequencies and modal shapes of the bridge and their participating masses. The first ten natural frequencies (Hz) calculated for the two proposed bridge models are listed in Table 2.

	Brick model (Model 1)				**Shell model (Model 2)**			
n°	ν [Hz]	mass x	mass y	mass z	ν [Hz]	mass x	mass y	mass z
1	2.18	0.002	**0.19**	5.9E-05	2.19	1.7E-04	**0.22**	2.6E-07
2	3.86	4.9E-04	2.5E-02	3.3E-04	4.09	4.2E-04	0.031	1.7E-06
3	4.94	**0.19**	2.8E-02	5.4E-04	5.12	**0.21**	1.8E-05	1.3E-04
4	5.21	2.4E-02	**0.16**	2.4E-06	5.57	4.6E-05	**0.24**	3.5E-07
5	6.56	0.009	5.1E-04	1.6E-03	6.68	0.022	3.3E-04	4E-05
6	6.84	3.6E-03	4.4E-04	9.4E-04	7.21	4E-04	3.3E-03	3.7E-06
7	7.86	2.7E-02	6.9E-02	1.5E-05	8.25	0.0127	0.085	1.1E-06
8	9.03	**0.22**	8.9E-03	1.4E-04	9.11	**0.23**	0.005	2E-04
9	9.71	8.9E-04	5.6E-05	2.4E-05	9.86	1.2E-05	5E-06	**0.13**
10	9.75	1.6E-05	2.0E-04	**0.12**	10.1	4E-05	0.002	7E-05

Table 2. The first ten natural frequencies (Hz) calculated for the two proposed bridge models.

The first eight vibration modes for the two models are quite similar. In particular, the mode shapes are the same, while the frequencies differ by less than 7%.

However, it can be observed that the participating masses associated with the fourth mode in the two models differ by more than 50%, while the 10th mode of Model 1 corresponds to the 9th in Model 2. Thus, the fully three-dimensional model is indeed able to capture more complex out-of-plane and torsional vibration modes. Model 2, however, enables accounting for the most important features of the bridge's dynamic behavior and, due to its low computational load, was chosen to perform the transient analysis, which is extremely onerous from the computational point of view.
Figure 9 shows the most significant mode shapes for Model 1.

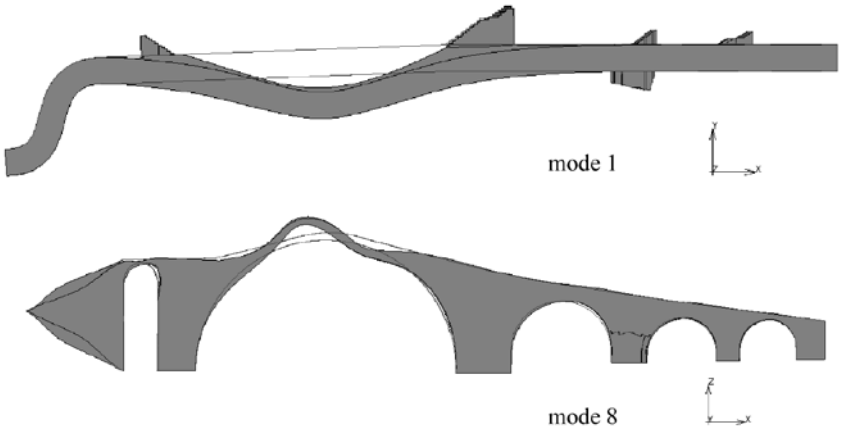

Figure 9. 1st and 8th mode shapes of Model 1.

2.3.2 Transient analysis

2.3.2.1 Input definition

The dynamic analyses were carried out on Model 2 by applying a three-component time-history acceleration to the base nodes. In particular, the three-dimensional accelerogram employed in the analysis was recorded in Fivizzano by the FIVI station during the earthquake of June 21th 2013, which struck the nearby area of Lunigiana (Tuscany) [16]. Figure 10 plots the three components along the East-West, North-South and Up-Down directions with a time step of 5E-3 s. The record's Peak Ground Acceleration (PGA) is 138 cm/s^2. The amplitudes have the same order of magnitude in the three directions, and the frequency content, which is the same for the two horizontal components, ranges from 1 to 8 Hz, affecting the first eight frequencies of the linear elastic models, while the vertical component involves the higher frequencies also. A seismic shaking duration of 12s has been used in all calculations. The material mechanical characteristics are once again those used for the static analysis and reported in Table 1.
The analysis runs were conducted first using the original accelerogram and then successively repeated with a base acceleration time-history amplified by a factor of 3 in order to emphasize the results and evaluate the bridge's seismic behavior under extreme conditions. All analyses were performed assuming the constituent materials

to exhibit masonry-like behavior, with zero tensile strength and limited compressive strength (3 MPa) and then repeated for the linear elastic case.

2.3.2.2 Results of the transient analysis

Figures 11 to 14 present the results of the transient analyses in terms of maximum relative displacements, minimum principal stresses and maximum principal fracture strains attained along the model's length during the entire seismic sequence. All figures refer to the middle plane of the shell elements. The dashed lines represent the nonlinear cases and the continuous lines represent the linear analysis results. The red lines mark the results for the case with input amplification (3x), whereas the blue lines refer to the unamplified case. The results for the bridge self-weight alone are indicated with a black dashed line. Figure 11 shows the maximum absolute values of the displacements of the bridge extrados with respect to the base attained during shaking.

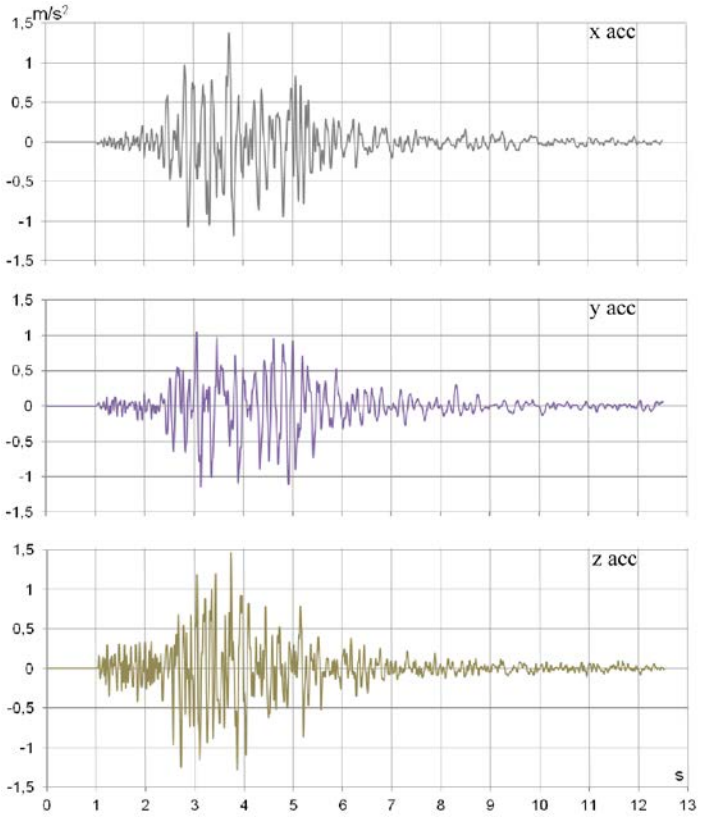

Figure 10. Time-histories of ground acceleration components recorded in Fivizzano by the FIVI station on June 21, 2013.

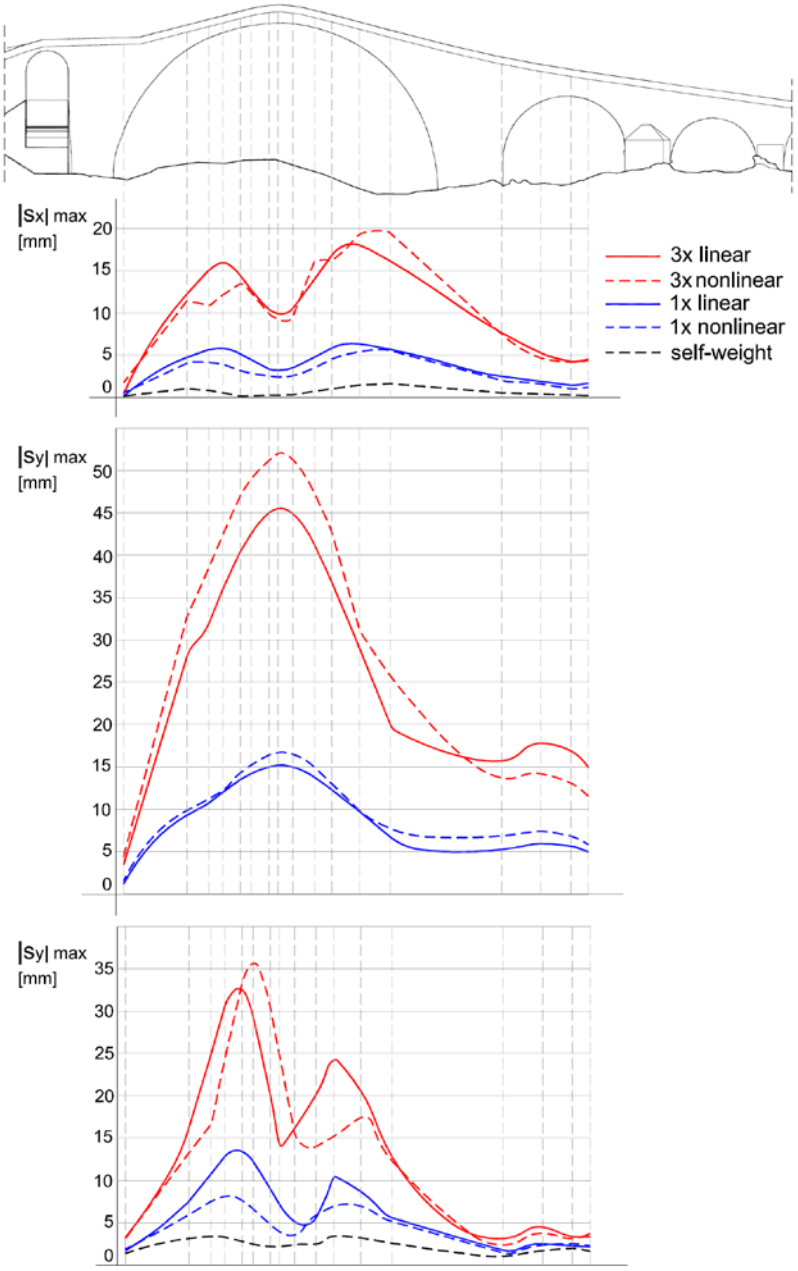

Figure 11. Maximum absolute displacements values at the bridge extrados with respect to the base in the three directions during seismic shaking.

It can be firstly observed that the largest displacements were found in the main span arch and in the out-of-plane (*y*) direction. However, the displacements in the other directions, especially along the *z* axis, are not negligible. This can be explained by the high values of the vertical earthquake component and the shape of the in-plane vibration modes, which exhibit marked vertical deflections (see Figure 9). Moreover, the *y*-displacements obtained in the nonlinear case are generally higher than in the linear case, though the resulting values differed by less than 10%.

Figures 12 and 13 show the absolute values of the minimum principal stresses attained during the shaking on the main arch's intrados and extrados, respectively. Note that only in the case of the amplified input was the material compressive strength reached and, in this case, the differences between the linear and nonlinear cases are obviously quite marked. The unamplified seismic acceleration also provoked a sizeable compressive stress increment with respect to the self-weight of up to about 200%, though nonlinearities in compression are not activated.
Figure 14 shows the maximum principal fracture strains values attained in the bridge's extrados during the shaking. As expected, the maximum fracture strains are concentrated in the central part of the main arch, where they can also be found under permanent loads (see Figure 5).

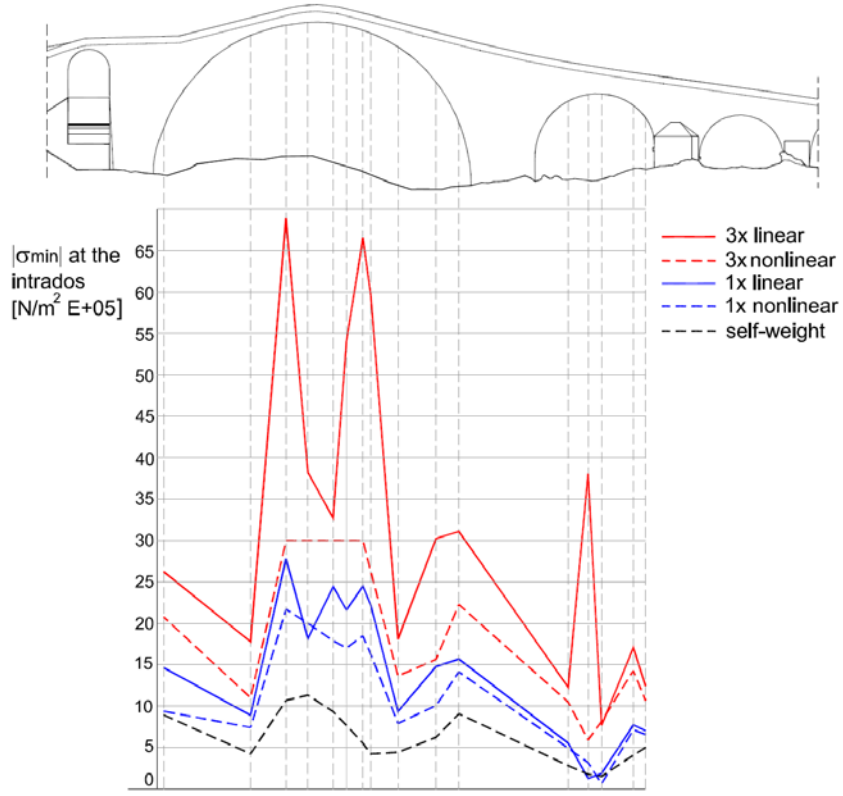

Figure 12. Absolute values of the minimum principal stress at the bridge intrados attained during the seismic shaking.

Figure 15 shows the relative *y*-displacements on the crown extrados of the main arch vs. time for both cases of amplified (red line) and unamplified (blue line) input, considering the materials' nonlinearity. It can be seen that the 3x amplified input results in displacements amplified by about a factor of 3 as well. However the two responses are out of phase, as a result of the nonlinear behavior.
Figure 16 shows the behavior of the principal minimum stress vs. time at node 1921, at the extrados of the main arch. It is noteworthy that in the case of the amplified input (red line), the material attains the limit strength in both tension and

compression. For this reason, the graph is asymmetrical with respect to the stress level induced by the bridge self-weight.

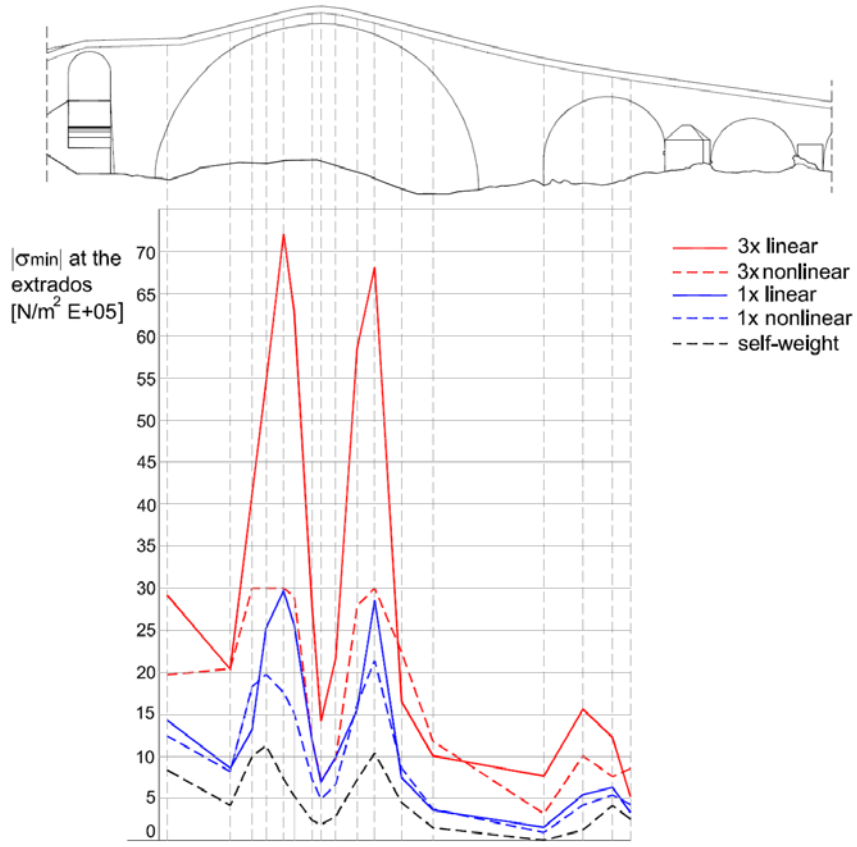

Figure 13. Absolute values of the minimum principal stress at the bridge extrados attained during the seismic shaking.

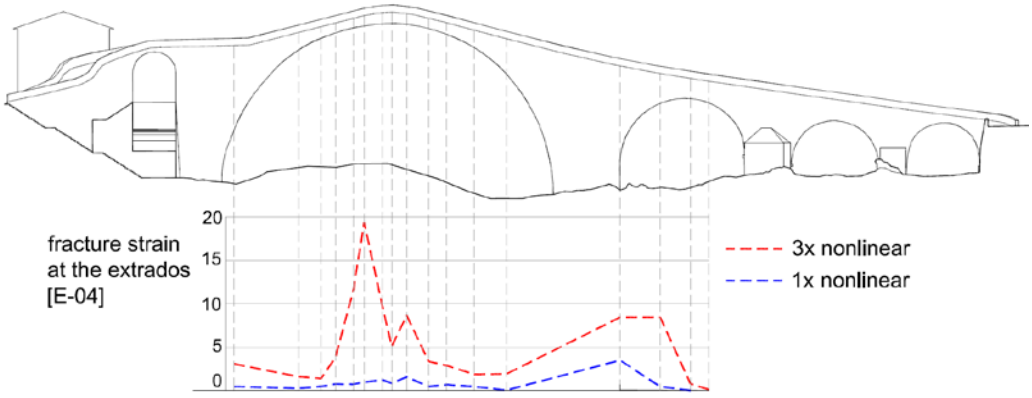

Figure 14. Maximum principal fracture strains at the bridge extrados attained during the seismic shaking.

Figure 17 represents the Discrete Fourier Transform (DFT) of the *y*-acceleration input and the *y*-acceleration responses for both the linear (continuous line) and nonlinear (dashed line) cases for the unamplified (blue diagram) and amplified (red

diagram) input. The significant DFT amplitudes in the figure are consistently within the range of 1 to 8 Hz. Note that in correspondence to modal frequencies 1 and 4 shown in Table 2 and representative of the bridge's out-of-plane motion, the DFT amplitudes are greatly accentuated in both the linear and nonlinear responses.

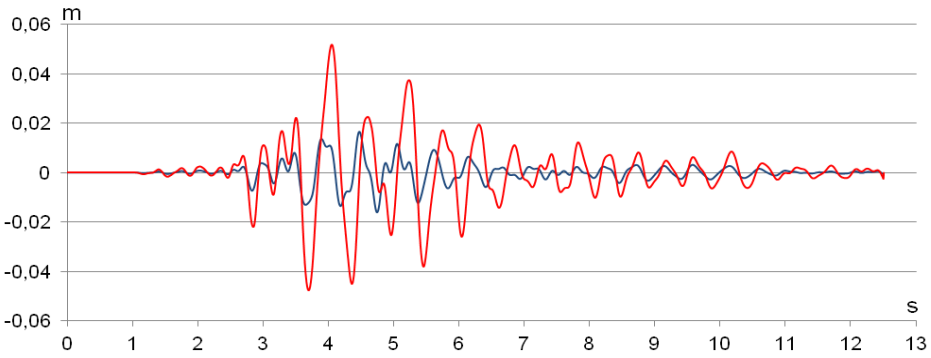

Figure 15. y-displacements of the main arch crown (node 2211) *vs.* time − nonlinear case. 3x amplified input (red line); unamplified input (blue line).

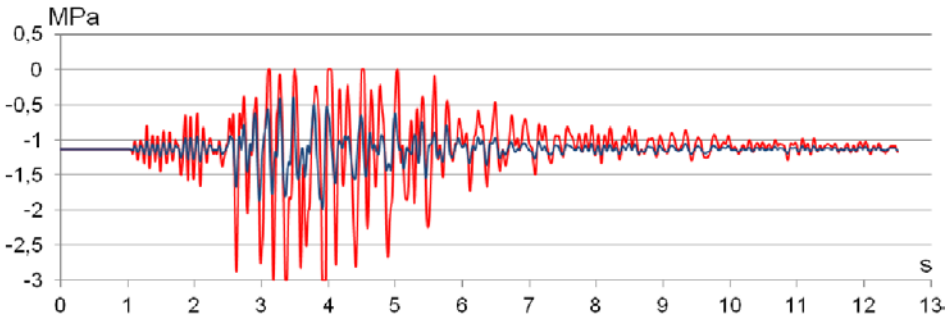

Figure 16. Minimum compressive stress *vs.* time on layer 6 of node 1921 at the extrados of the main arch in the nonlinear case. 3x amplified input (red line); unamplified input (blue line).

However, the material's nonlinearity causes a reduction in the amplitudes, particularly evident around frequency 1 (Table 2), and amplification of the lower frequencies response.

Figure 18 shows the DFT of the structure's *x*-responses in both the linear and nonlinear cases with amplified and unamplified input. In this direction the reduction in DFT amplitudes for the nonlinear response is already evident in the unamplified case. This can be explained by the presence, even for the self-weight alone, of fracture strains acting within the plane of the structure. The phenomenon is revealed between 5 and 6 Hz.

The DFT of the *z*-response, shown in Figure 19, highlights a certain amplification of the higher frequencies, over 10 Hz, with similar values for the linear and nonlinear cases.

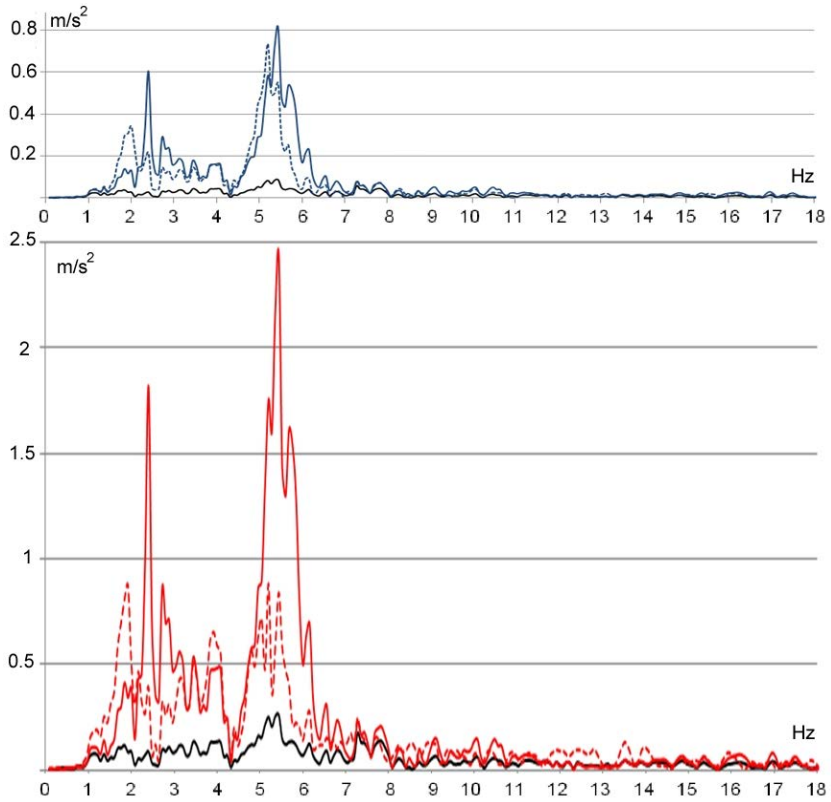

Figure 17. DFT of the *y*-acceleration responses at the crown (node 2211). 3x amplified input (red diagram); unamplified input (blue diagram). Input at the base (black line); response in the linear (continuous line) and nonlinear (dashed line) case.

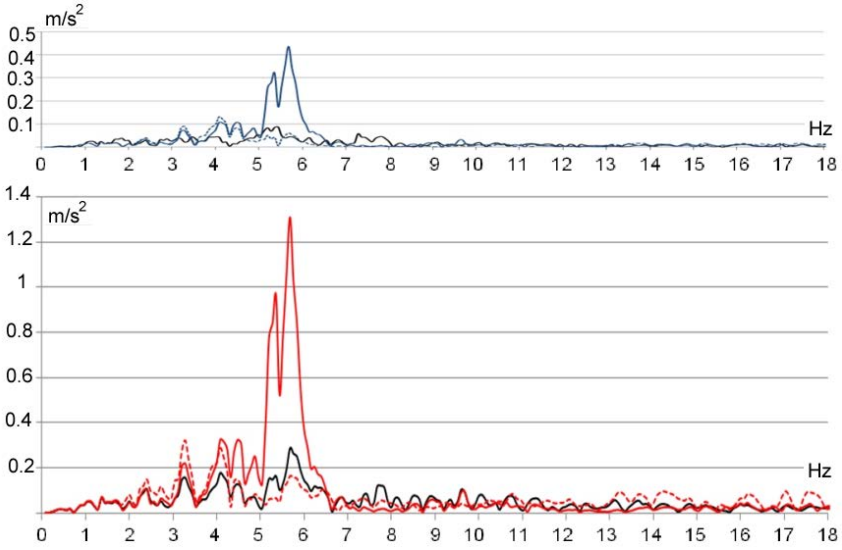

Figure 18. DFT of the *x*-acceleration responses at the crown (node 2211). 3x amplified input (red diagram); unamplified input (blue diagram). Input at the base (black line); response in the linear (continuous line) and nonlinear (dashed line) case.

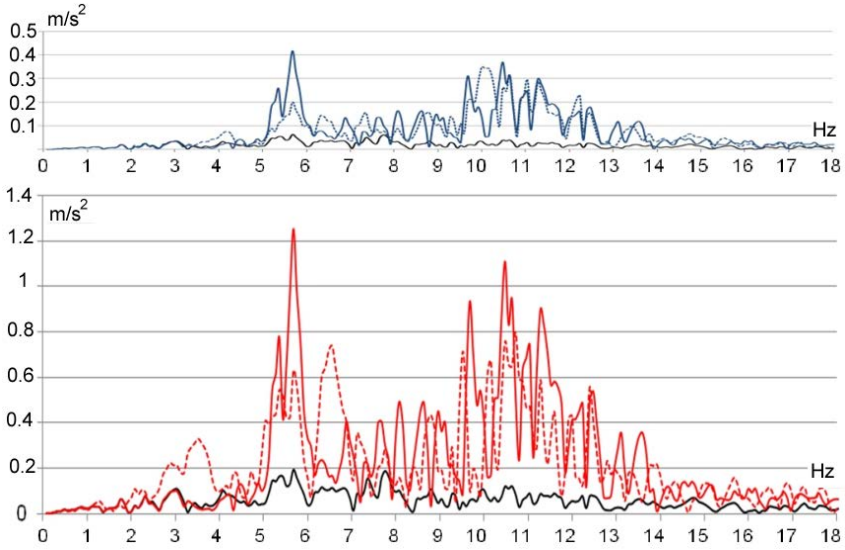

Figure 19. DFT of the *z*-acceleration responses at the crown (node 2211). 3x amplified input (red diagram); unamplified input (blue diagram). Input at the base (black line); response in the linear (continuous line) and nonlinear (dashed line) case.

Conclusions

The paper reports on the results of a structural analysis and evaluation of the static and seismic behavior of the Maddalena bridge in Borgo a Mozzano. The analysis has been conducted via the NOSA-ITACA code by modeling masonry as a nonlinear elastic material with no tensile strength and limited compressive strength. The bridge is studied under both its self-weight alone and a base acceleration time-history taken from the records of the June 21, 2013 earthquake in Lunigiana. Moreover, in order to assess the dynamic behavior of the structure under extreme conditions, further analyses were also conducted using the original accelerogram amplified by a factor of three.

The static analysis highlights the good response of the bridge under its self-weight alone, with compression levels far below the limit values. With regard to the dynamic analyses, the differences between the linear and nonlinear responses have been analyzed in terms of displacements, stress level and frequency content. During the seismic shaking the model enters the nonlinear range in areas where nonlinearities are already triggered by the self-weight alone. Furthermore, the material's nonlinear behavior, on the one hand, alters the frequency content of the structural response and, on the other, reduces the stress state with respect to the linear case, especially when the base acceleration is amplified.

In conclusion, the modeling indicates a wide safety margin of the structure under static and dynamic actions. Further development is still necessary in order to support more efficient, meaningful interpretations of the analysis results and improve detection of masonry damage. However, by neglecting any form of dissipation apart

from viscous damping, the constitutive equation of masonry-like material enables arriving at a generally precautionary estimate of the structure's dynamic response.

Acknowledgements. This research has been supported by the Region of Tuscany (project "Tools for modelling and assessing the structural behaviour of ancient constructions: the NOSA-ITACA code", PAR FAS 2007-2013). This support is gratefully acknowledged.

References

[1] N. Gucci, A. De Falco, Il Fascino e la Funzione, "Il Ponte della Maddalena detto del diavolo". Maria Pacini Fazzi Editore, Lucca, 2010.

[2] http://www.nosaitaca.it/en/

[3] M. Lucchesi, C. Padovani, G. Pasquinelli and N. Zani, "Masonry constructions: mechanical models and numerical applications". Lecture Notes in Applied and Computational Mechanics Vol. 39, Springer-Verlag, Berlin Heidelberg, 2008.

[4] http://www.salome-platform.org/

[5] G. Del Piero, "Constitutive equation and compatibility of the external loads for linearly-elastic masonry-like materials", Meccanica, 24 pp.150-162, 1989.

[6] S. Di Pasquale, "New trends in the analysis of masonry structures", Meccanica, 27, pp. 173-184, 1992.

[7] S. Degl'Innocenti, C. Padovani and G. Pasquinelli, "Numerical methods for the dynamic analysis of masonry structures". Structural Engineering and Mechanics, 22, pp.107-130, 2006.

[8] M. Porcelli, V. Binante, M. Girardi, C. Padovani and G. Pasquinelli, "A solution procedure for constrained eigenvalue problems and its application within the structural finite-element code NOSA-ITACA", Calcolo, Springer, Online First 29 March 2014.

[9] M. Girardi, C. Padovani and G. Pasquinelli, "Numerical modelling of the static and seismic behaviour of historical buildings: the church of San Francesco in Lucca", in B.H.V. Topping, P. Iványi, (Editors), "Proceedings of the Fourteenth International Conference on Civil, Structural and Environmental Engineering Computing", Civil-Comp Press, Stirlingshire, UK, Paper 80, 2013. doi:10.4203/ccp.102.80.

[10] V. Binante, S. Briccoli Bati, M. Girardi, M. Lucchesi, C. Padovani and D. Pellegrini, "A Case Study for the NOSA-ITACA Project: the "Voltone" in Livorno", in B.H.V. Topping, P. Iványi, (Editors), "Proceedings of the Fourteenth International Conference on Civil, Structural and Environmental Engineering Computing", Civil-Comp Press, Stirlingshire, UK, Paper 79, 2013. doi:10.4203/ccp.102.79

[11] G. Angelini G., A. De Falco, M. Lucchesi and D. Pellegrini, "Studio della cupola del duomo di Massa Marittima", SAFE MONUMENTS Workshop - Tra Conservazione e Sicurezza di Edifici Monumentali e del Costruito Storico, Florence, 28 March 2014.

[12] M. Callieri, M. Corsini, M. Girardi, C. Padovani, A. Pagni, G. Pasquinelli and R. Scopigno, “The “Rognosa” Tower in San Gimignano: digital acquisition and structural analysis”, in B.H.V. Topping, J.M. Adam, F.J. Pallarés, R. Bru, M.L. Romero, (Editors), "Proceedings of the Tenth International Conference on Computational Structures Technology", Civil-Comp Press, Stirlingshire, UK, Paper 138, 2010. doi:10.4203/ccp.93.138

[13] M. Girardi, M. Lucchesi, C. Padovani, B. Pintucchi, G. Pasquinelli and N. Zani, “Numerical methods for slender masonry structures: a comparative study”, in B.H.V. Topping, (Editor), "Proceedings of the Eleventh International Conference on Computational Structures Technology", Civil-Comp Press, Stirlingshire, UK, Paper 118, 2012. doi:10.4203/ccp.99.118

[14] M. Girardi, “On the dynamic behaviour of masonry beam-columns: an analitycal approach”, European Journal of Mechanics A-Solids, 45, pp. 174-184, 2014.

[15] R.W. Clough and J. Penzien, "Dynamics of structures", McGraw-Hill, 1975.

[16] http://itaca.mi.ingv.it/